

Characterizing Electrical Noise

Jack Macaulay (20222474)

Group Members: Noah Kriss and Liam Gallagher

Submitted on 07/02/2024 for ENPH453

Contents

1	Introduction and Theory	1
1.1	Aperiodic vs Periodic Noise	1
1.2	Types of Electrical Noise	1
1.3	Lock-In Amplifiers	3
2	Apparatus	4
2.1	Equipment	4
2.2	Setup	4
2.2.1	Single-Ended Mode	4
2.2.2	Differential Mode	5
2.2.3	Cryostat Setup	6
2.2.4	LabView Interface	6
3	Procedure	8
3.1	Determination of Termination	8
3.2	Sensitivity Sweep	8
3.3	Time Constant	9
3.4	Final Values	10
4	Data Analysis	12
4.1	Error Propagation	12
4.2	Single-Ended Mode	12
4.3	Differential Mode	14
4.4	Cryostat	15
4.5	Additional Uncertainties	16
5	Results	18
5.1	Single-Ended Mode	18
5.2	Differential Mode	19
5.3	Cryostat	19
6	Discussion	20
7	Conclusion	21
	References	22

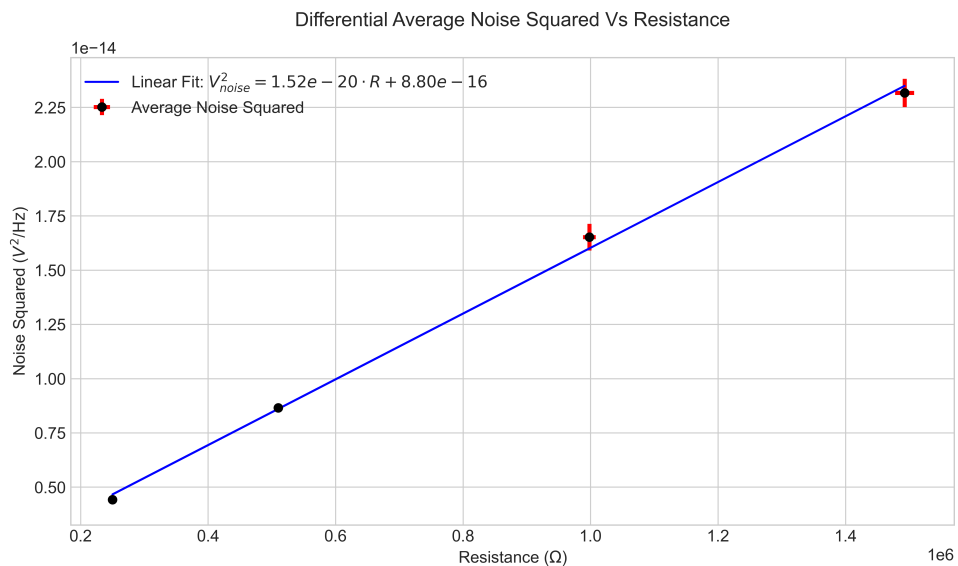
List of Figures

1	Plot outlining how different forms of noise may appear	2
2	Plot of thermal noise power spectral density from 0 - 2.5 MHz for $T = 22.5^\circ \text{ C}$	3
3	Sketch outlining connections for single-mode measurements. Resistor connected to channel A, function generator connected to reference on the lock-in amplifier.	5
4	Differential mode measuring setup. Resistor is connected across both measurement channels instead of one. All connections are made with female to female BNC cables.	6
5	Photograph of the LabView configuration used for collecting cryostat data.	7
6	Comparison of the power spectral density for terminators with differing material and impedance.	8
7	Plot showing different PSD profiles for 50Ω , room temperature with varying lock-in amplifier sensitivities.	9
8	Plotting noise spectrum for 50Ω terminator, 100 nV sensitivity over different time constants.	10
9	Initial plot for 10 nV sensitivity and 10 ms time constant at $T = 22.5^\circ \text{ C}$. Curves have nearly no flat region and odd roll-off.	10
10	Single-ended measurement sweep done at $T = 22.5^\circ \text{ C}$ with theoretical thermal noise values.	13
11	Single-ended measurement sweep linear region corresponding to thermal noise with theoretical calculations.	14
12	Differential measurement sweep. Two vertical lines to indicate linear region corresponding to thermal noise. Dashed lines are theoretical thermal noise calculations.	14
13	Differential measurement sweep over limited frequency bandwidth. Dashed lines correspond to theoretical predictions.	15
14	Cryostat with theoretical comparison. Note for theoretical comparison the temperature was estimated based on the experimental data. This was done using the single-ended measurement mode.	16
15	Linear region from cryostat data.	16
16	Average Noise squared against resistance for linear region of single-ended measurements.	18
17	Average Noise squared against resistance for linear region of differential measurements.	19

Executive Summary

Noise complicates electronic measurements, posing challenges for signal analysis. This study explores thermal noise in resistors using a lock-in amplifier for phase-sensitive detection. We systemically investigated thermal noise across different resistors, varying lock-in amplifier settings and using a cryostat for low-temperature studies.

A significant outcome was the empirical determination of Boltzmann's constant, measured at $(1.28 \pm 0.04) \times 10^{-23}$ J/K, with a percent error of $(7.15 \pm 0.23)\%$. This underscores the effectiveness of the lock-in amplifier in noise analysis. The value was extracted from the plot below which shows the average noise squared against the resistance. This experiment demonstrates the utility of phase-sensitive detection techniques. Further research could explore additional manifestations of electrical noise, such as flicker or dielectric noise.



Abstract

In virtually every measurement process, noise is an unavoidable phenomenon that can obscure or distort the signal of interest. This is particularly true in the field of electronics, where accurate data acquisition is paramount. The primary aim of this laboratory exercise was to delve into the nature and characteristics of thermal noise within resistors, a fundamental aspect of electronic noise. Utilizing a lock-in amplifier, we systematically investigated thermal noise across various resistors. Our experimental setup utilized the different lock-in amplifier measurement modes alongside a cryostat for low temperature experimentation. Through this we experimentally determined Boltzmann's constant, yielding a value of $(1.28 \pm 0.04) \times 10^{-23}$ J/K, with a percent error of $(7.15 \pm 0.23)\%$. The findings of this study not only contribute to a deeper understanding of noise in electronic components but also exemplify the application of phase-sensitive detection techniques in quantifying fundamental constants.

1 Introduction and Theory

In experimental research, accurately distinguishing between the signal and noise is critical for data interpretation. "Noise" refers to the unpredictable variations in a measured physical quantity that do not correlate with the expected behavior, defined as the "signal" [1]. The distinction impacts the accuracy, precision, and validity of experimental findings and is a universal challenge across all fields of scientific inquiry.

Noise, in its various forms, is inherent in experimental setups and can provide insights into underlying physical processes. For example, the analysis of electrical noise in semiconductors can reveal details about material properties and charge carrier dynamics, offering a deeper understanding of the physical processes at play [1].

Among the different types of noise (see Section 1.2), this report focuses on thermal noise, also known as Johnson-Nyquist noise. Thermal noise originates from the random motion of charge carriers due to thermal energy within a conductor and is a fundamental consideration in the analysis of electronic systems [1].

1.1 Aperiodic vs Periodic Noise

Mathematically, a measured signal, can be expressed as the sum of the desired signal and the noise (refer to equation 1).

$$S(t) = S_{\text{desired}}(t) + N(t) \quad (1)$$

Noise can manifest itself as either periodic or aperiodic disturbances. Periodic noise consists of disturbances that exhibit a regular, repeating pattern over time. Typically, periodic noise can be traced back to deterministic sources, such as the clock signal in digital circuits, which introduce periodic interference into the measured signal.

Aperiodic noise, on the other hand, lacks regularity and predictability. It arises from stochastic processes that produce random fluctuations in the signal. A prime example of this is thermal noise which is described by thermal agitation in conductive materials. To better analyze aperiodic noise, it is common practice to examine the signal in the frequency domain, achieved by applying a Fourier transform:

$$F(\omega) = \int_{-\infty}^{\infty} f(t)e^{-j\omega t} dt \quad (2)$$

The Fourier transform facilitates the decomposition of the signal into its constituent frequencies, providing a spectrum that reveals the distribution of noise power across frequencies [1].

1.2 Types of Electrical Noise

This report explores electrical noise which in itself is aperiodic. Electrical noise appears in various forms, such as shot noise, dielectric noise, flicker noise and thermal noise, each of which contribute uniquely to the noise profile of electronic devices.

Shot noise arises from the discrete nature of electric charge carriers (such as electrons or holes). It is characterized by the random statistical fluctuations of current due to the

discrete and random arrival of the charge carriers [2]. Dielectric noise arises from the thermal agitation of dipole moments within dielectric material. This agitation causes fluctuations in the material's polarization, subsequently inducing voltage fluctuations across electronic components [1].

Flicker noise (or '1/f' noise) is a form of noise that is more prominent at low frequencies. The underlying causes of flicker noise can vary widely, ranging from trap dynamics to mobility fluctuations within semiconductor materials [3]. The figure below (refer to figure 1) illustrates how different form of noise may appear in a spectrum.

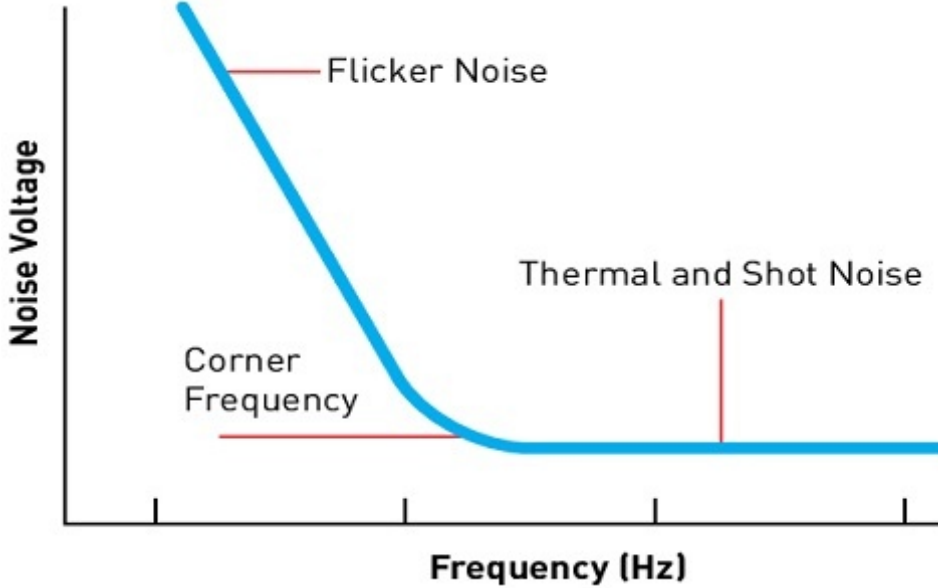


Figure 1: Plot showing noise spectrum and different manifestations of electrical noise. Note 1/f dominates at low frequencies [4].

Thermal noise in a resistor, arises from fluctuations in the local population of free charge carriers and their random motion due to thermal exchange with its surroundings. This interplay of fluctuations in charge carrier population and random motion results in a fluctuating net image charge across the resistor terminals, effectively creating voltage noise. The fundamental equation describing thermal noise in a resistor is:

$$V_{\text{noise}}^2 = 4kTR\Delta f \quad (3)$$

Where V_{noise}^2 is the mean square noise voltage across the resistor, k is Boltzmann's constant, T is the temperature, R is the resistance, and Δf is the equivalent noise bandwidth [5].

The spectral density $S_V(f)$ of thermal noise is given by:

$$S_V(f) = 4kTR \quad (4)$$

The power spectral density (PSD) of thermal noise is independent of frequency, indicating that it is "white" noise with a constant amplitude across a frequency spectrum [5]. Figure 2 illustrates the theoretical PSD for a range of resistor values that were tested experimentally (refer to Data Analysis).

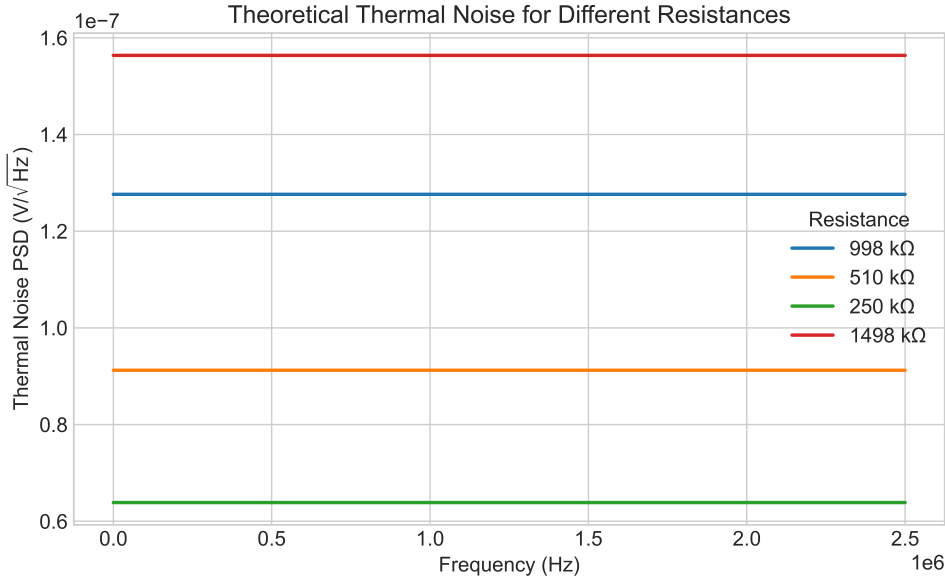


Figure 2: Plot of thermal noise power spectral density from 0 - 2.5 MHz for $T = 22.5^\circ \text{ C}$.

1.3 Lock-In Amplifiers

Lock-in amplifiers play a crucial role in noise analysis and signal processing, particularly in experimental physics where extracting a clear signal from a noisy background is required.

A lock-in amplifier is designed to detect and measure the amplitude and phase of a signal at a specific reference frequency, effectively filtering out noise that is not coherent with the reference. This is achieved through "phase-sensitive detection", where the incoming signal $S(t)$ is multiplied by a reference signal $R(t)$ that oscillates at the desired frequency. The product is then passed through a low-pass filter, yielding the component of $S(t)$ that is in phase with $R(t)$ (refer to equation below) [6].

$$D(t) = S(t) \cdot R(t) \cdot \cos(\phi) \quad (5)$$

Where ϕ is the phase difference between the input and reference signals. This output is then integrated over a period significantly longer than the inverse of the lowest frequency of interest, effectively averaging out all components that are not at the reference frequency. The result is a measure of the signal's power at the reference frequency [6].

By systematically varying the reference frequency and repeating the measurement, the lock-in amplifier constructs a PSD profile of the signal, constructing a profile over a range of frequencies. The PSD is instrumental in identifying various types of noise, such as thermal noise as discussed previously [6].

The lock-in amplifier has two important parameters - the time constant and sensitivity. The time constant (τ sets the bandwidth over which the signal is averaged. A longer time constant can provide better noise reduction at the cost of a slower response to changes in the signal. Sensitivity refers to the minimum input signal amplitude that can be accurately measured above the noise level. The sensitivity setting adjusts the gain of the amplifier; a higher sensitivity means that smaller signals can be detected, but it also means the amplifier is more susceptible to being saturated by larger signals [6].

2 Apparatus

2.1 Equipment

The following instruments and components were used to conduct this experiment.

1. Stanford Research Systems SR810 DSP Lock-in Amplifier
2. Agilent 33220A Function Generator
3. LabView Interface
4. 2 x Female BNC-BNC Cable (50 Ω impedance, 20" long, and 50 Ω impedance, 12" long)
5. Carbon Composition Resistors (1 M Ω \pm 5%, 510 k Ω \pm 5%, 250 k Ω \pm 5%, 1498.5 k Ω \pm 5%)
6. 0 Ω , 50 Ω metal, and 50 Ω rubber terminator plugs
7. Cryostat with 998 M Ω resistor
8. Liquid Nitrogen
9. Traceable Calibration Control Company Thermometer (accurate to within 0.1° C)
10. Velleman DVM850BL multi-meter

2.2 Setup

Three distinct configurations were employed to investigate thermal noise. Each configuration utilized a LabView interface, all of which are explained below:

2.2.1 Single-Ended Mode

Single-ended measurements follow the schematic shown in the image below (refer to Figure 3).

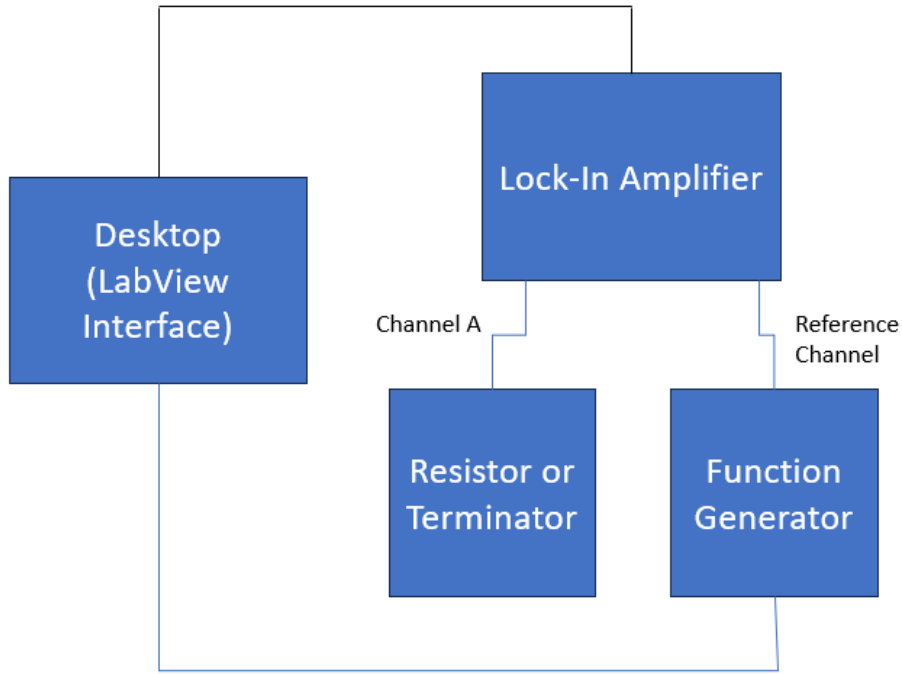


Figure 3: Sketch outlining connections for single-mode measurements. Resistor connected to channel A, function generator connected to reference on the lock-in amplifier.

In single-ended measurements the ground serves as the reference for measurements. This simplicity; however, introduces a vulnerability to ground-induced noise. Any disturbance present on the ground line will inadvertently become superimposed on the measured signal.

2.2.2 Differential Mode

Differential measurements involve using two inputs of the lock-in amplifier to measure the voltage difference across the component of interest (refer to figure 4).

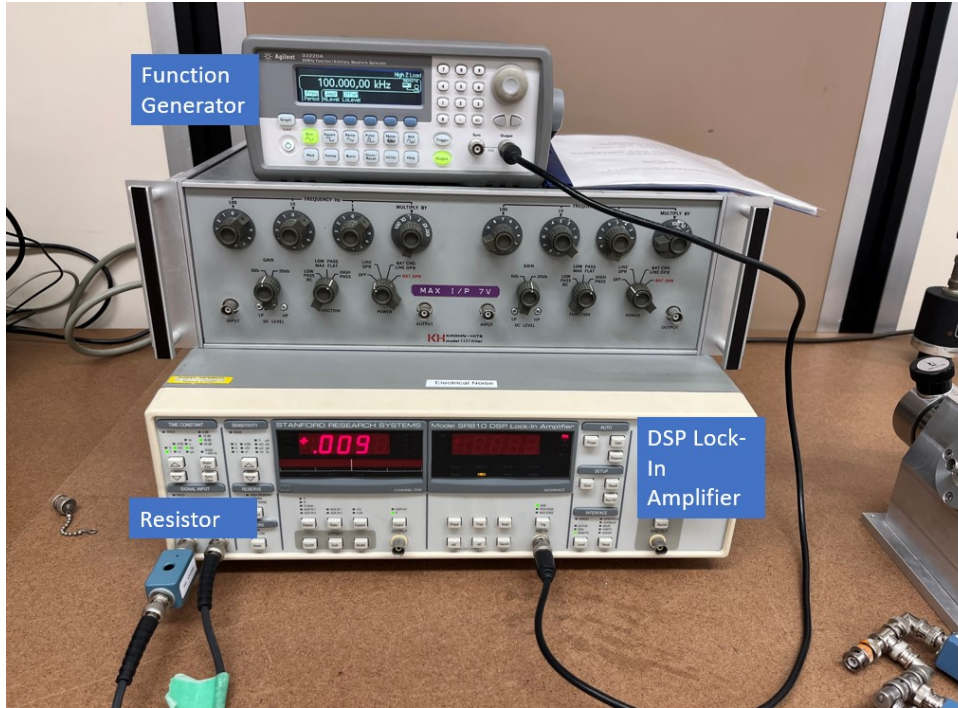


Figure 4: Differential mode measuring setup. Resistor is connected across both measurement channels instead of one. All connections are made with female to female BNC cables.

Unlike the single-ended mode, neither input is grounded in this configuration. Instead, the lock-in amplifier measures the difference between the two channels, cancelling out common-mode noise.

2.2.3 Cryostat Setup

The third setup introduces a cryostat, housing a $1 \text{ M}\Omega$ resistor, allowing for an in-depth exploration of the interplay between temperature and thermal noise. This setup was identical to the single-ended measurement schematic, with the addition of a BNC cable connecting the cryostat to the single input. Liquid nitrogen serves as the cooling agent for this setup.

2.2.4 LabView Interface

Below is an image of the LabView interface which was facilitated data acquisition and the function generator frequency sweep (refer to figure 5).

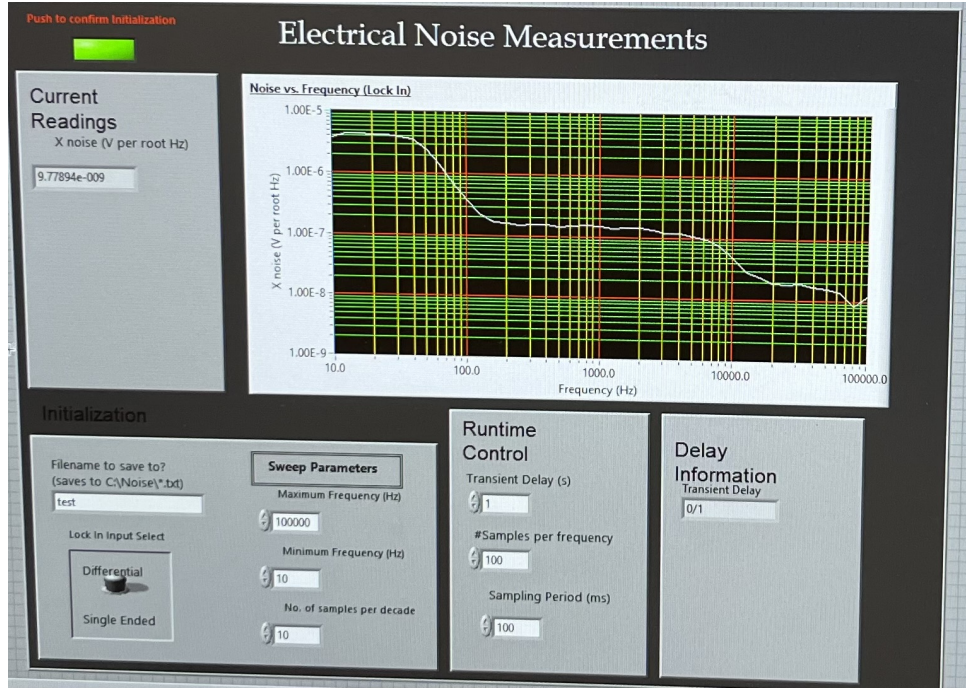


Figure 5: Photograph of the LabView configuration used for collecting cryostat data.

Starting from the leftmost panel, measurements could be taken either using the differential or single-ended setting. The frequency band and number of samples per decade were set to 10 - 10,000 Hz and 10 samples per decade respectively. This allowed us to capture a large enough frequency range to see different forms of noise.

The runtime control panel accounted for the transient delay, samples per frequency, and sampling period. Transient delay refers to the time it takes before measurements are taken again (i.e., after the frequency is changed). Samples per frequency determines the number of points averaged per frequency value. The sampling period determines the interval between consecutive data points. These parameters were set to 1 s, 100 samples/frequency, and 100 ms respectively.

3 Procedure

Prior to gathering report-quality data, tests were conducted to determine the appropriate terminator, sensitivity, and time-constant.

3.1 Determination of Termination

The objective of this test was to determine which terminator. There were three terminators tested: a $0\ \Omega$ bare terminator, $50\ \Omega$ metal and $50\ \Omega$ rubber terminator. Below is a plot showing the power spectrum for each of the terminators (refer to figure 6).

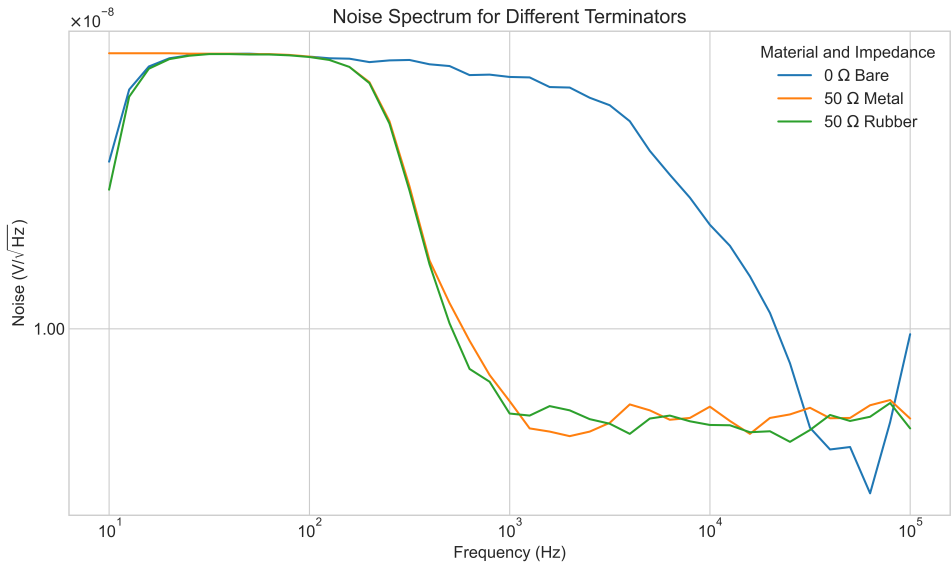


Figure 6: Comparison of the power spectral density for terminators with differing material and impedance.

The metal and rubber terminators showed similar performance. Following discussion with Professor Park subsequent tests used the rubber terminator. For this test the settings were as follows: 1 second transient delay, 10 points per octave, 10 points per frequency, 100 nV sensitivity and 18 dB/octave slope.

3.2 Sensitivity Sweep

The optimal sensitivity was found by using a rubber terminator and going through all the sensitivities on the lock-in amplifier. Below is a plot showing that behaviour (refer to figure 7).

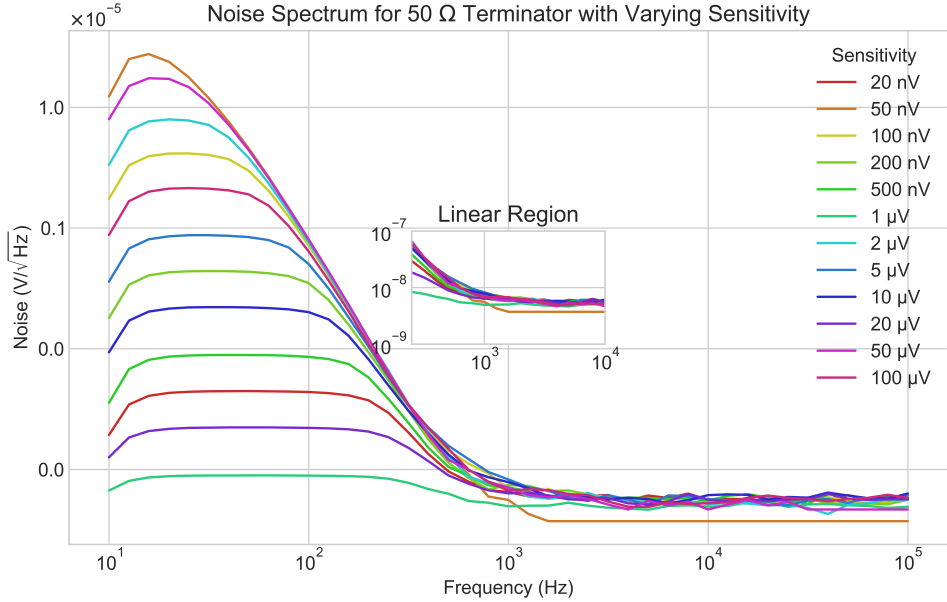


Figure 7: Plot showing different PSD profiles for 50Ω , room temperature with varying lock-in amplifier sensitivities.

Evidently many of the curves appear quite similar, and the linear portion is hard to distinguish. However, 100 nV stood out as a strong candidate due its smooth and flat region and as such we chose to go forward with that value.

3.3 Time Constant

To further optimize noise analysis, the same procedure was conducted for time constants. The selection criteria for the optimal time constant included a balance between a well-defined linear region (i.e., thermal and shot noise) and smooth roll-off characteristic in the low-frequency range (i.e. $1/f$). Below is a plot showing the noise spectrum of a 50Ω terminator measured at a sensitivity of 100 nV (refer to figure 8)

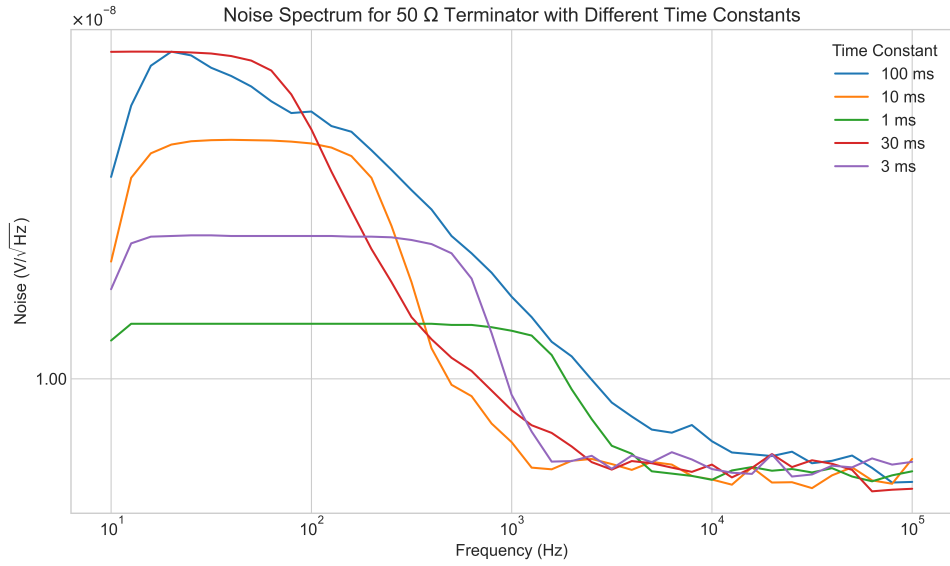


Figure 8: Plotting noise spectrum for 50Ω terminator, 100 nV sensitivity over different time constants.

The time constant of 10 ms (orange line), exhibited an extended linear region alongside a nice roll-off. Consequently, 10 ms was established as the standard for subsequent measurements.

3.4 Final Values

After establishing values for the sensitivity and the time constant, noise spectrum analysis tests were conducted on different resistors. The primary results were quite poor (refer to figure 9).

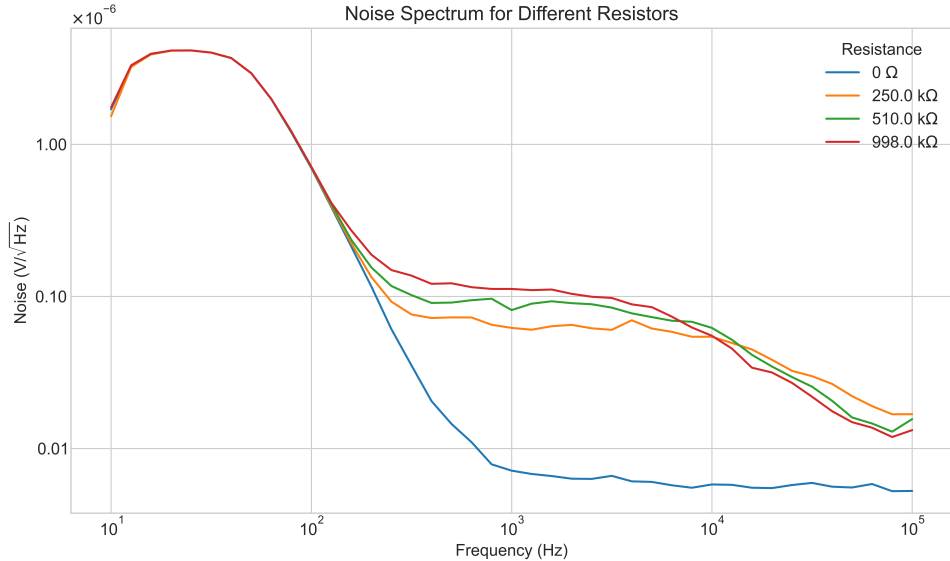


Figure 9: Initial plot for 10 nV sensitivity and 10 ms time constant at $T = 22.5^\circ C$. Curves have nearly no flat region and odd roll-off.

Following discussion with Professor Park, the underlying issue was that the termina-

tors vs testing resistors varied by several orders of magnitude (i.e., $50\ \Omega$ vs $250\ k\Omega$) and our sensitivity was too small. It was recommended to proceed with a sensitivity of $10\ \mu V$.

There are two other settings (slope and reserve) that were qualitatively justified. The slope setting refers to the roll-off rate of the low-pass filter. A steeper slope means the filter will more sharply attenuate frequencies outside the cutoff frequency. From preliminary testing, $18\ dB/octave$ performed the best. The reserve setting relates to the lock-in amplifier's ability to maintain performance in the presence of large signals that may otherwise overload it. Low reserve makes sense for settings where there is lower variation in signal strength. Hence, we went forward with low reserve. The final lock-in amplifier parameters are shown below (refer to 1)

Parameter	Value
Time Constant	$10\ ms$
Sensitivity	$10\ \mu V$
Slope	$18\ dB/Octave$
Reserve	Low Noise

Table 1: Optimal Lock-In Amplifier Parameters.

4 Data Analysis

This section provides a comprehensive overview and analysis of the data collected for the different testing setups.

4.1 Error Propagation

Prior to discussing experimental findings, it is important to go over the propagation of uncertainties in the measurement of noise. Since this report focuses on thermal noise, error propagation will only be mentioned in the context of thermal noise. Based on the power spectral density equation, uncertainties lie in the measurements of R and T . Assuming these uncertainties are independent, the variance in $S_v(f)$, denoted as $\sigma_{S_v}^2$, can be determined by the error propagation formula:

$$\sigma_{S_v}^2 = \left(\frac{\partial S_v}{\partial R} \right)^2 \sigma_R^2 + \left(\frac{\partial S_v}{\partial T} \right)^2 \sigma_T^2$$

where σ_R and σ_T represent the uncertainty of the resistance and temperature measurements, respectively. The partial derivatives of $S_v(f)$ with respect to R and T are:

$$\begin{aligned} \frac{\partial S_v}{\partial R} &= 4kT \\ \frac{\partial S_v}{\partial T} &= 4kR \end{aligned}$$

Substituting these derivatives back into the error propagation formula yields:

$$\sigma_{S_v}^2 = (4kT)^2 \sigma_R^2 + (4kR)^2 \sigma_T^2$$

The thermometer performed readings to within 0.1° C and the multi meter has a 1% uncertainty.

4.2 Single-Ended Mode

The first test was conducted across four resistors in the single-ended measuring mode. Below is a plot of the initial results (refer to figure 10). Note that the lack of uncertainty bars is not meant to mean there are no uncertainties - this is discussed further in this section.

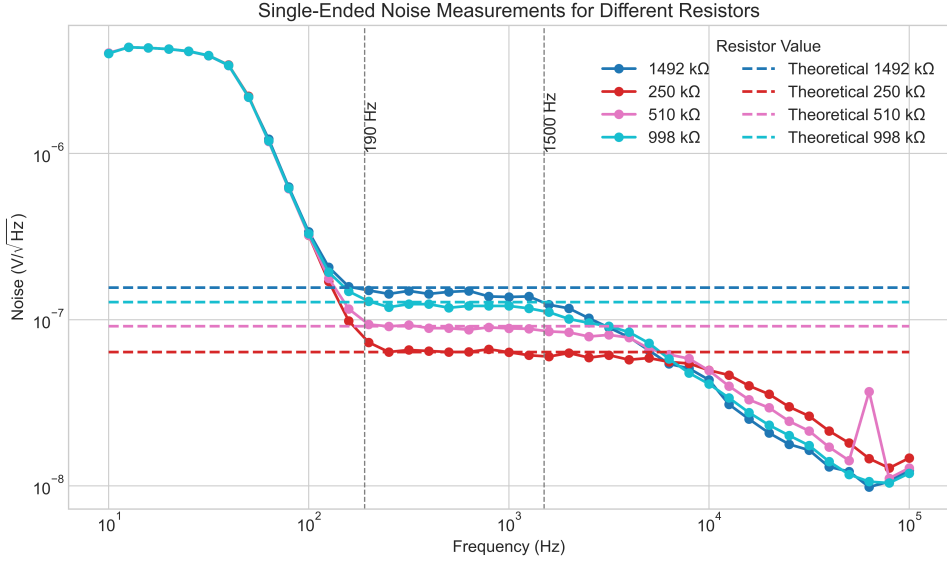


Figure 10: Single-ended measurement sweep done at $T = 22.5^\circ \text{ C}$ with theoretical thermal noise values.

In the plot above, there are three distinct bands as separated by the vertical lines at 190 Hz and 1500 Hz. The band from 0 – 190 Hz corresponds to flicker noise and visually has a $1/f$ roll-off. The second region between 190 – 1500 Hz corresponds to thermal noise which is the focus of this report. To establish an appropriate region to study, several bandwidths were explored, and upon visual inspection 190 – 1500 Hz provided the most reasonable looking linear region. After 1500 Hz, theory predicts that the spectrum should still be flat (i.e., white); however it clear is not. In the high-frequency domain, noise behaviour becomes atypical. Beyond the threshold corresponding to the electron transit time across the diode gap, electron trajectories are influenced by neighbouring charges in transit, leading to a reduction in noise levels.

To study thermal noise better, the 190 – 1500 Hz bandwidth was used. Below is a plot showing said bandwidth, with error calculations as discussed above and the theoretical benchmark for comparison (refer to figure 11).

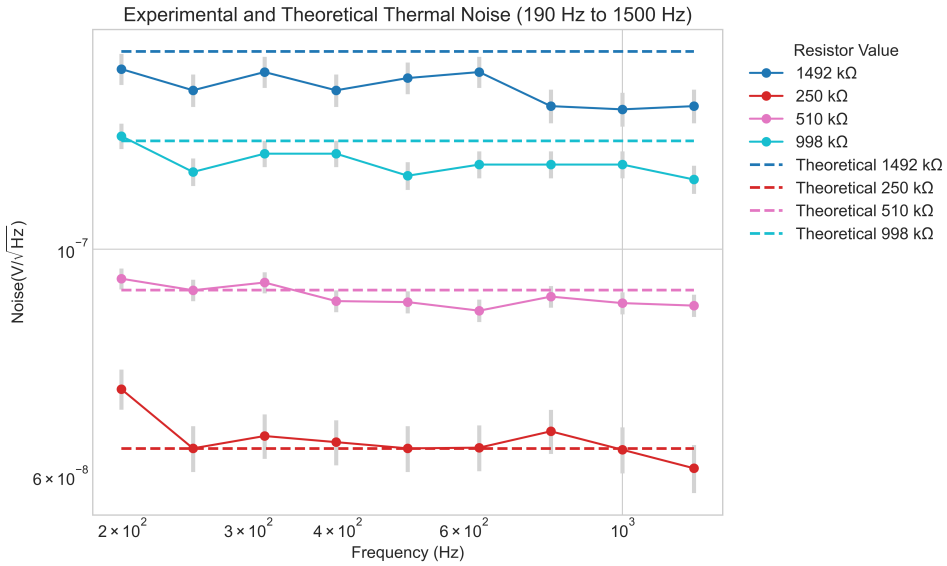


Figure 11: Single-ended measurement sweep linear region corresponding to thermal noise with theoretical calculations.

From the plot above, the 250 and 510 k Ω resistors match the theory within error. However, the 998 and 1492 k Ω do not match within error but visually are reasonably close.

4.3 Differential Mode

The second test was the same as the first one; however, conducted using the differential measuring schematic. As discussed the same bands appear; however, the thermal noise band appears to be much longer (i.e. 190-2000 Hz instead of 190-1500 Hz). This suggests that between 1500-2000 Hz there was some common-mode noise. The plot with theoretical thermal noise predictions is shown below (refer to 12).

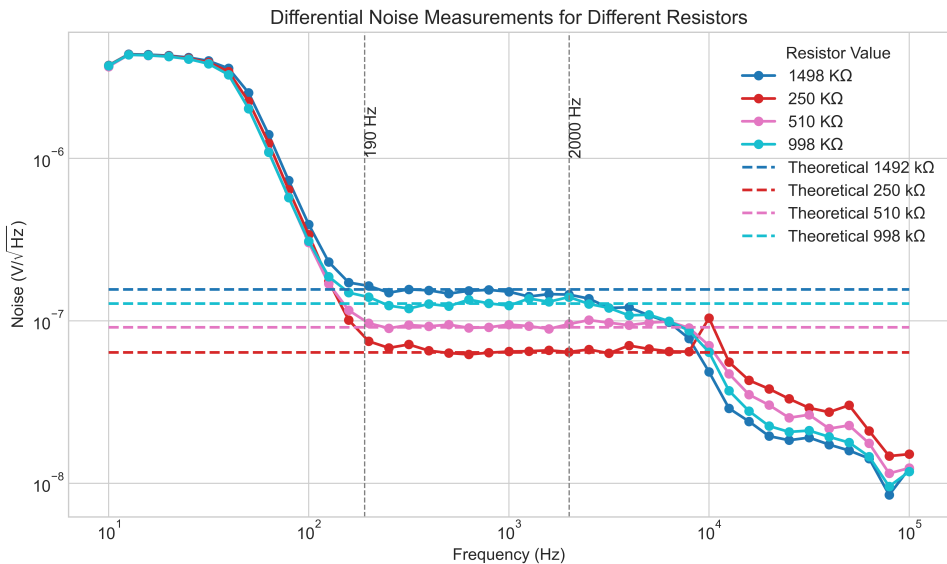


Figure 12: Differential measurement sweep. Two vertical lines to indicate linear region corresponding to thermal noise. Dashed lines are theoretical thermal noise calculations.

Similar to the analysis above, below is a zoomed in plot of the noise response - from 190 to 2000 Hz (refer to figure 13).

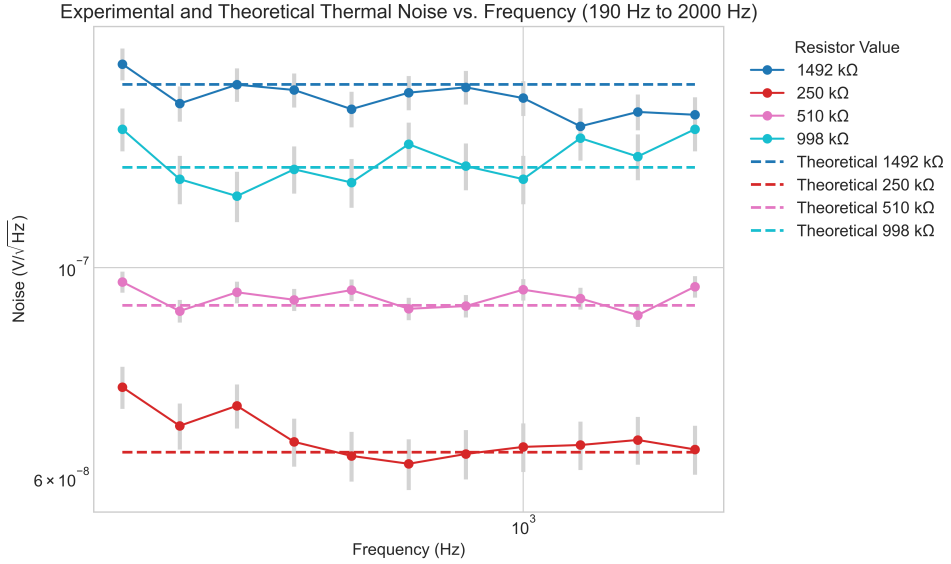


Figure 13: Differential measurement sweep over limited frequency bandwidth. Dashed lines correspond to theoretical predictions.

Notice that in this plot all resistor values match the theory within error and exhibit thermal noise properties over a larger frequency range. This is likely due to common-mode noise interfering with single-ended measurements leading to poorer results.

4.4 Cryostat

For the cryostat data, there was no accurate way of measuring the temperature making the theoretical prediction/comparison quite difficult. To do so, I plotted the data and varied the temperature until I visually had a reasonable result. This was a means for estimating temperature. In the future having a device capable of measuring such low temperatures would make this a smoother process. Below is a plot of the data (refer to figure 14).

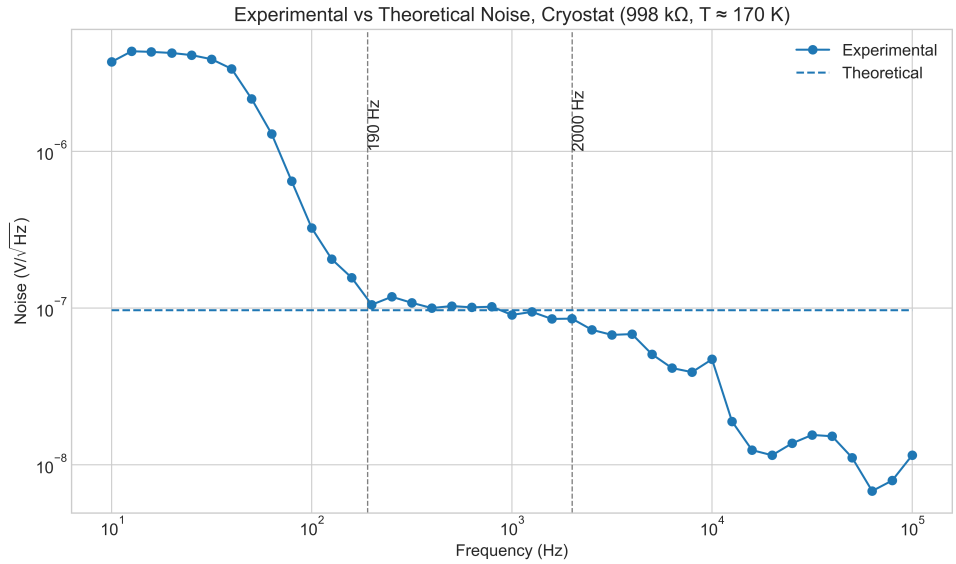


Figure 14: Cryostat with theoretical comparison. Note for theoretical comparison the temperature was estimated based on the experimental data. This was done using the single-ended measurement mode.

This plot has similar tendencies to all other plots shown, the major difference is that the theoretical plot is estimated and could not be validated due to inability to read temperature. The linear region is shown below, using the error calculations discussed prior (without including temperature) it seems to match the theoretical data reasonably well (refer to figure 15).

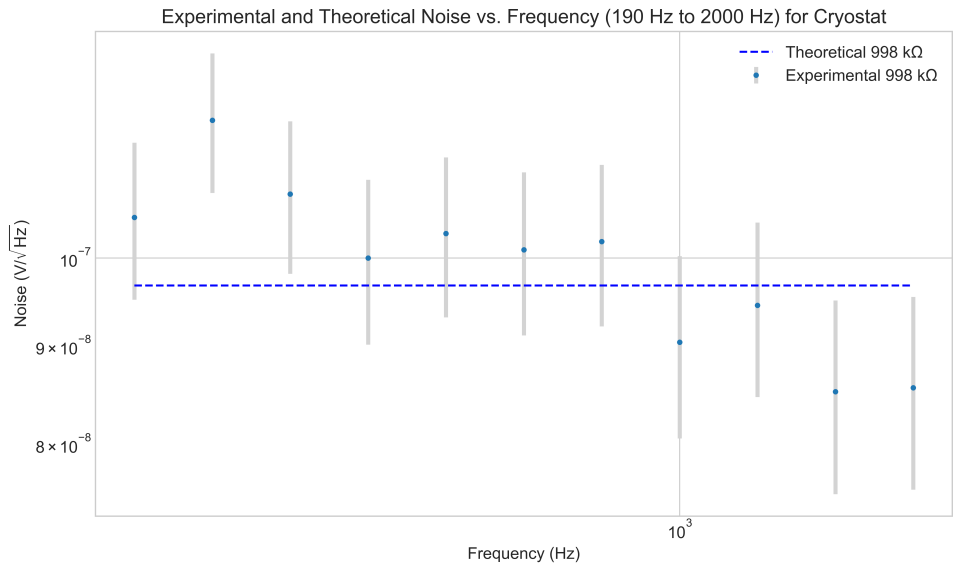


Figure 15: Linear region from cryostat data.

4.5 Additional Uncertainties

In addition to temperature and resistance uncertainties, other sources contribute to measurement inaccuracies. Each noise point averages 100 measurements from the lock-in

amplifier, implying a standard deviation for each point. However, due to time constraints, this was not implemented in the LabView interface. Furthermore, the function generator introduces uncertainties in amplitude and frequency generation. Different frequency bands have different accuracy, but these were not accounted for due to time limitations. Other electromagnetic sources from various labs around the fifth floor could have introduced additional noise; however, these could not be systematically accounted for.

5 Results

In this section, the data from above will be further analyzed to determine Boltzmann's constant. The linear region is described by the power spectral density equation previously mentioned. By plotting the noise squared against resistance the slope takes the form:

$$V_{\text{noise}}^2/R = \frac{k}{4T} \quad (6)$$

Thus the slope divided by $4T$ should approximately be Boltzmann's constant.

The uncertainty is the average noise squared is calculated from the standard error of the mean of the noise measurements. The standard error mean noise was calculated as follows:

$$SEM_{\bar{V}} = \frac{\sigma_V}{\sqrt{N}} \quad (7)$$

Where N is the number of measurements and σ_V is the standard deviation. The average noise squared mean error was calculated using:

$$\Delta(\bar{V}^2) = 2 \cdot \bar{V} \cdot SEM_{\bar{V}} \quad (8)$$

The uncertainty along the x-axis is the 1% error in the multimeter measurements.

5.1 Single-Ended Mode

Following the procedure described above, below is a plot of the single-ended mode average noise square as a function of resistance (refer to figure 16).

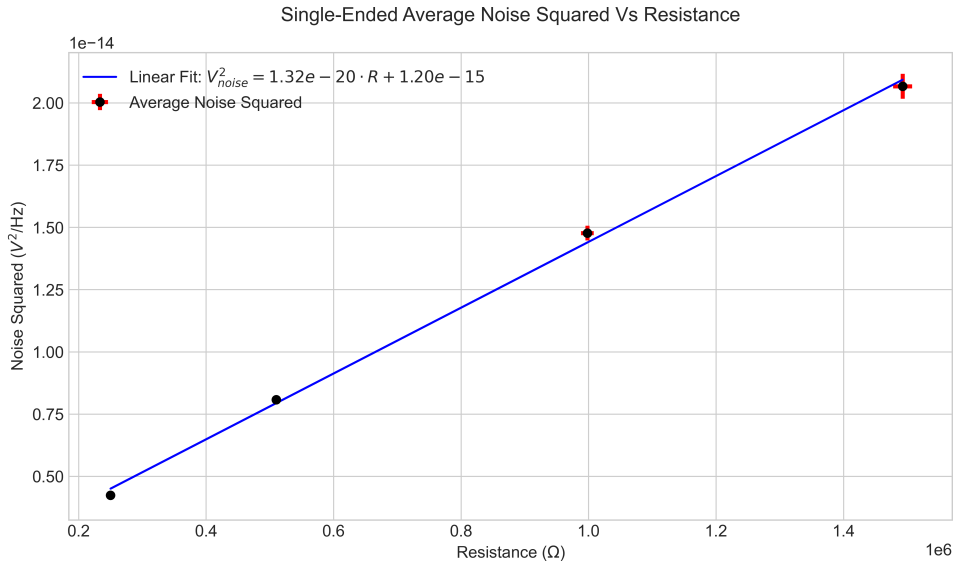


Figure 16: Average Noise squared against resistance for linear region of single-ended measurements.

In this plot, the slope is 1.32×10^{-20} , which corresponds to an experimental Boltzmann's constant of $(1.12 \pm 0.34) \times 10^{-23}$ J/K and a percent error of $(19.01 \pm 3.08)\%$. The final results for the single-ended measurements are shown in the table below.

Table 2: Comparison of Theoretical and Experimental Single-Ended Noise Measurements

	Resistor Value			
	250 kΩ	510 kΩ	998 kΩ	1492 kΩ
Theoretical [V/√Hz]	6.39×10^{-8}	9.12×10^{-8}	1.28×10^{-7}	1.56×10^{-7}
Experimental [V/√Hz]	$6.52 \times 10^{-8} \pm 1.10 \times 10^{-9}$	$8.99 \times 10^{-8} \pm 7.32 \times 10^{-10}$	$1.22 \times 10^{-7} \pm 1.23 \times 10^{-9}$	$1.44 \times 10^{-7} \pm 1.74 \times 10^{-9}$

5.2 Differential Mode

Repeating the same procedure for differential measurements yields the plot below (refer to figure 17).

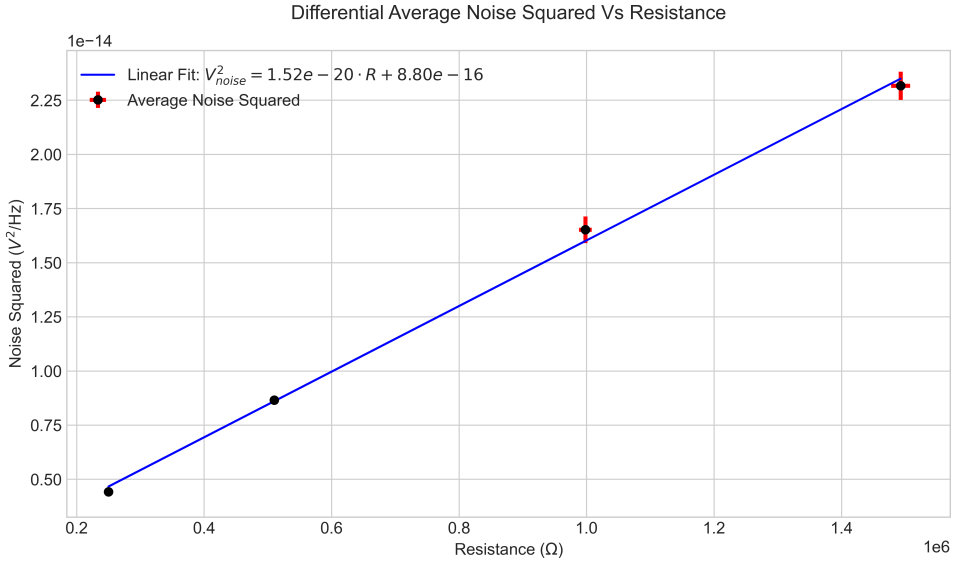


Figure 17: Average Noise squared against resistance for linear region of differential measurements.

From this plot Boltzmann's constant was found to be $(1.28 \times 10^{-23}) \pm 4.18 \times 10^{-23}$ J/K which corresponds to a percent error of $(7.15 \pm 0.23)\%$.

Table 3: Comparison of Theoretical and Experimental Single-Ended Noise Measurements

	Resistor Value			
	250 kΩ	510 kΩ	998 kΩ	1492 kΩ
Theoretical [V/√Hz]	6.39×10^{-8}	9.12×10^{-8}	1.28×10^{-7}	1.56×10^{-7}
Experimental [V/√Hz]	$6.62 \times 10^{-8} \pm 1.15 \times 10^{-9}$	$9.29 \times 10^{-8} \pm 7.45 \times 10^{-10}$	$1.30 \times 10^{-7} \pm 2.19 \times 10^{-9}$	$1.51 \times 10^{-7} \pm 1.92 \times 10^{-9}$

5.3 Cryostat

For the cryostat since there is only one value, the only value that could be extracted was the average noise. The experimental noise was $(9.93 \times 10^{-08}) \pm 2.97 \times 10^{-9}$ V/√Hz, compared to the theoretical value of 9.68×10^{-08} V/√Hz giving a 2.65% error. This values matches quite well with the theory; however, this is not a reliable number. Since the temperature could not be accurately measured, I experimented with different temperatures until I saw a reasonable fit.

6 Discussion

The experimental investigation yielded some interesting results. The effectiveness of the lock-in amplifier in isolating and analyzing noise components was evident in both the single-ended and differential measurement modes. The single-ended mode had greater error, and the theoretical data did not line up very well with the experimental results, especially for higher valued resistors. This highlighted the prominence of common-mode noise. Whereas the differential mode, which eliminates common-mode noise performed quite well and matched the theoretical values to a higher degree of precision.

The presence of a linear region in all datasets reaffirmed the fundamental nature of thermal noise as described by Johnson-Nyquist theory. The extended linear region indicates lock-in amplifier's ability to isolate noise components. Alongside the longer linear region (corresponding to thermal noise), the differential measurements yielded a significantly better approximation of Boltzmann's constant.

Several factors contributed to the uncertainties in the experimental results, including the limited accuracy of the thermometer, the unknown standard deviation in noise measurements due to averaging, and uncertainties intrinsic to the electronic devices present. Additionally, electromagnetic influence from other sources around the fifth floor such as other experiments, although difficult to quantify, cannot be disregarded. In the future, a temperature measuring device with a broader range and greater accuracy would be very helpful, alongside a standard deviation calculation inside the LabView program.

7 Conclusion

The experimental exploration of electrical noise, provided valuable insights into the behaviour of noise in electronic components and the influence of temperature on noise characteristics. The use of both single-ended and differential measurement modes showcased the presence of common-mode noise which resulted in poor single-ended mode data.

The experimental determination of Boltzmann's constant as $(1.28 \pm 0.04) \times 10^{-23}$ J/K, with a percent error of $(7.15 \pm 0.23)\%$ emphasized the practicality behind noise analysis (i.e, being able to experimentally show a constant). Alongside, the precision of using a lock-in amplifier for phase-sensitive detection. It is worth noting that the resistor noise is likely not solely a byproduct of thermal agitation but could also encompass other forms of noise that were not accounted for. However, for the purposes of this lab, and the data analyzed - the experimental and theoretical thermal noise values match quite well.

Future work could aim to refine the experimental setup, particularly improving temperature measurement accuracy in cryostat trials and minimizing external noise. Additionally, testing more resistors inside the cryostat would help us better understand and validate the cryostat data we have (e.g., allow us to find Boltzmann's constant). Given further time, it would be interesting to explore other forms of noise, such as flicker and shot noise which would help provide a more comprehensive understanding of the data present.

Overall, this experiment demonstrated the utility of noise analysis, offering a practical approach to investigating fundamental properties of electronic components and the underlying physical processes that contribute to noise.

References

- [1] Advanced Physics Laboratory, *Electrical Noise*, Winter 2018, laboratory Manual.
- [2] D. R. Paschotta, “Shot noise,” https://www.rp-photonics.com/shot_noise.html.
- [3] Cadence, “1/f noise: Flicker noise impact and mitigation strategies,” <https://resourcespcb.cadence.com/blog/2023-1-f-noise-flicker-noise-impact-and-mitigation-strategies>, 2023.
- [4] ElProCus, “An overview of flicker noise in electrical circuits,” <https://www.elprocus.com/flicker-noise/>.
- [5] M. Sayer and A. Mansingh, *Signal to Noise Considerations*. Prentice-Hall India, 2000, queen’s U Engin. & Science Library QC39 .S29 2000t.
- [6] Stanford Research Systems, *SR810 DSP Lock-In Amplifier*, 1st ed., Stanford Research Systems, Sunnyvale, California, January 2005, revision 1.8. [Online]. Available: www.thinkSRS.com